Available online at www.sciencedirect.com
ScienceDirect
Ceramics International 35 (2009) 1757–1768
CERAMICS INTERNATIONAL
www.elsevier.com/locate/ceramint

Combustion synthesis of high-performance $Li_4Ti_5O_{12}$ for secondary Li-ion battery

Tao Yuan [a], Rui Cai [a], Ke Wang [a], Ran Ran [a], Shaomin Liu [b], Zongping Shao [a,*]

[a] State Key Laboratory of Materials-Oriented Chemical Engineering, Nanjing University of Technology, No. 5 Xin Mofan Road, Nanjing 210009, PR China
[b] The Australian Research Council (ARC) Center for Functional Nanomaterials, School of Engineering, The University of Queensland, Brisbane, QLD 4072, Australia

Received 8 July 2008; received in revised form 16 August 2008; accepted 1 October 2008
Available online 21 October 2008

Abstract

Spinel $Li_4Ti_5O_{12}$ was synthesized by a simple glycine-nitrate auto-combustion by applying aqueous medium and constricting the reactions in the pores of cellulose fibers. The products from the auto-combustion and further calcination at various temperatures were characterized by XRD, SEM, BET surface area and TEM examinations. Pure phase and well-crystallized nano-$Li_4Ti_5O_{12}$ oxides were obtained at a calcination temperature of 700 °C or higher. The 700 °C calcined one shows the best and high electrochemical performance, which reached a capacity of ~125 mAh/g at 10 C discharge rate with fairly stable cycling performance even at 40 °C. Electrochemical impedance spectroscopy tests demonstrated that the surface reaction kinetics of $Li_4Ti_5O_{12}$ was improved significantly with the increase of its electronic conductivity.

Keywords: $Li_4Ti_5O_{12}$; Combustion synthesis; Cellulose; Rate capacity

1. Introduction

Nowadays, there are great interests in rechargeable batteries for application in hybrid electric vehicles and as renewable or dispersed energy storage systems, which typically require higher charge/discharge rates and bigger battery sizes, and emphasize more on the price, rate capacity and safety of the batteries. Rechargeable lithium-ion batteries are promising candidates due to its high energy and power densities [1–3]. State-of-the-art lithium secondary batteries compose of a graphite/carbon-related anode [4–6], which has serious safety concerns for large-size applications. On the other hand, due to the low lithium intercalating voltage of approximately 100 mV (vs. Li/Li^+), highly reactive metallic lithium forms easily under fast charge rate, which will deposit on the surface of electrode particles and has the high risk to react with the electrolyte or highly charged cathodes. Furthermore, graphite/carbon-based anodes also suffer from a lack of a clear end-of-charge indicator in their voltage profiles [1].

Recently, spinel-related $Li_4Ti_5O_{12}$ oxide, or written as $Li[Li_{1/3}Ti_{5/3}]O_4$, has been studied as an alternative candidate of anode in solid, liquid and gel Li-ion batteries [7–12]. It is cheap, and more importantly, features a unique lithium insertion/extraction mechanism that involves two phases (spinel $Li_4Ti_5O_{12}$ and rocksalt-type $Li_7Ti_5O_{12}$) having the same symmetry with near zero change in the unit cell volume during the charge/discharge processes [13–18]. Such characteristics ensure an excellent cycling performance with a long cycling life. Moreover, it offers a discharge platform around 1.55 V versus Li^+/Li, above the reduction potential of most organic electrolytes, consequently passive films with high resistances from the reduction of electrolytes (SEI) can be avoided on the $Li_4Ti_5O_{12}$ surface [19,20]. This voltage is also sufficiently high for avoiding the formation of metallic lithium.

The main obstacle of $Li_4Ti_5O_{12}$ is, however, its poor rate capacity. One effective way for the rate-performance enhancement is to reduce its particle size. Smaller particle size means shorter diffusion length and higher surface reaction sites, which would lead to improved lithium intercalation kinetics [21–33]. On the other hand, the surface modification is also effective for enhancing the surface reaction kinetics. Various kinds of surface coatings, such as oxides, carbon materials, polymers

* Corresponding author. Tel.: +86 25 83587722; fax: +86 25 83365813.
E-mail address: shaozp@njut.edu.cn (Z. Shao).

0272-8842/$34.00
doi:10.1016/j.ceramint.2008.10.010

and conductive agents, have been exploited [34–38]. The low electronic conductivity of $Li_4Ti_5O_{12}$ accounts in part for its poor rate performance. The doping strategy, on the purpose of improving the bulk electronic conductivity, and therefore, the performance of the anode at high charge/discharge rate, has also been extensively exploited [39–44].

So far, the spinel-type $Li_4Ti_5O_{12}$ was mainly prepared by solid-state reactions of mechanically mixed anatase-type TiO_2 and Li_2CO_3 or LiOH [7,13,15,16,45]. The reaction is usually conducted at 800–1000 °C for prolonged time. However, the long-distance diffusion during the solid-state reaction of the reactants results in low homogeneity, irregular morphology, big particle sizes, and poor control of stoichiometry of the product. Compared with the solid-state reaction, the methods of wet chemical synthesis such as sol–gel, emulsion–gel and hydrothermal can obviously reduce the temperature of the reaction. Thus, the particle size was decreased significantly and the electrochemical properties of their productions was improved accordingly [21–33]. It is noticeable that such wet chemical synthesis methods always require a non-aqueous medium, which, however, increases the cost. Furthermore, the crystallographic structure usually grows poorly at low calcination temperature. Recently, Raja et al. introduced a novel aqueous combustion technique using an amino acid alanine as fuel to synthesize nano-crystalline $Li_4Ti_5O_{12}$. However, a pure phase of $Li_4Ti_5O_{12}$ cannot be obtained even after calcined at 800 °C for 10 h [46].

In this study, we report the synthesis of nano-sized $Li_4Ti_5O_{12}$ powders via a facile glycine-nitrate combustion process by applying an aqueous medium and constricting the reactions within the pores of cellulose fibers (cellulose–GN process). Pure phase and well-crystallized $Li_4Ti_5O_{12}$ oxides were obtained at calcination temperature as low as 700 °C. The as-derived anodes show excellent performance, especially, at high charge/discharge rate. Such nano-$Li_4Ti_5O_{12}$ anode will applied to high power lithium ion battery.

2. Experimental

2.1. Materials synthesis

The synthesis procedure of $Li_4Ti_5O_{12}$ powder is shown schematically in Fig. 1. The de-waxed cotton was applied as the cellulose fiber [47–49]. It was immersed in 67 wt.% concentrated nitric acid for a certain time, and then washed with de-ionized water to remove the free HNO_3 and dried at ~100 °C to form the activated cellulose fiber. The synthesis of $Li_4Ti_5O_{12}$ is described as follows. Tetrbutyl titanate [$Ti(C_4H_9O)_4$] was slowly dropped into de-ionized water under ice-water bathing and vigorous stirring leading to the formation of white precipitate of $TiO(OH)_2$. Nitric acid was then introduced under stirring to result in a transparent titanyl nitrate solution. Stoichiometric amount of $LiNO_3$ was added in, followed by the introduction of glycine as the fuel at the mole ratio of glycine: total metal ions of 3:1. The mixed solution was slowly soaked into the activated cellulose. After drying at 80 °C for several hours, the precursor was heated at 250 °C in an electrical oven to start the auto combustion. Fluffy $Li_4Ti_5O_{12}$ primary product was obtained, which has the morphological shape of the initial cellulose fiber and can be ground easily to fine powders. The primary was then further calcined at temperature between 500 and 900 °C for 5 h in air.

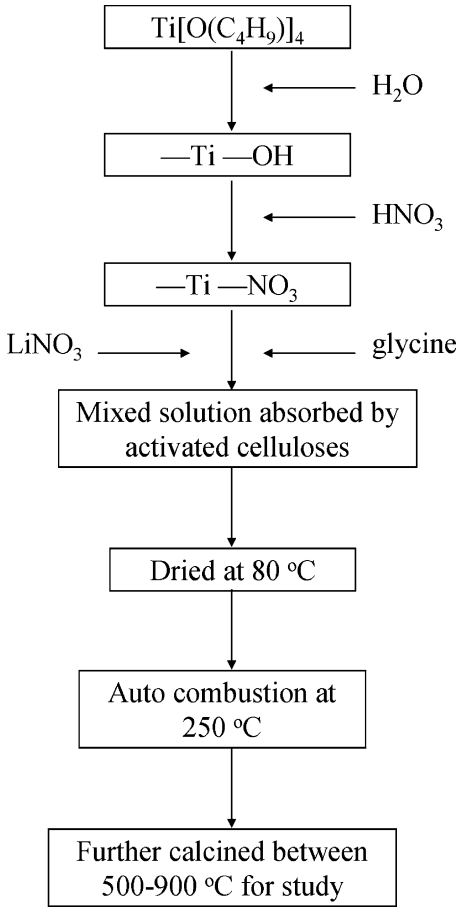

Fig. 1. A flow-chart for the synthesis of $Li_4Ti_5O_{12}$ via the cellulose-based combustion process.

Furthermore, as contrast, the $Li_4Ti_5O_{12}$ was also prepared by the solid-state route. The starting materials, Li_2CO_3 (AR) and TiO_2 (anatase), were mixed by simple milling. Excess Li was provided to compensate for the loss of Li during synthesis. Samples were heated in a muffle furnace at various temperatures in order to form pure $Li_4Ti_5O_{12}$ powders.

2.2. Electrode fabrication

The cells are based on the configuration of Li metal(−)|electrolyte| $Li_4Ti_5O_{12}$ (+) with a liquid electrolyte (1 M solution of $LiPF_6$ in ethylene carbonate (EC)-dimethyl carbonate (DMC) 1:1 in v/v). Microporous polypropylene film (Celgard, 2400) was used as the separator.

The working electrode was prepared from a paste of 85 wt.% $Li_4Ti_5O_{12}$ with 10 wt.% conductive Super P (NCM HERSBIT Chemical Co. Ltd., China) and 5 wt.% LA-132 binder (Chengdu Organic Chemicals Co. Ltd., China) in de-ionized water to make viscous slurries for efficient deposition. The slurries were deposited on current collectors of copper foil (10 μm) by blading, which was pretreated by etching with 1 M

nitric acid solutions followed by rinsing with water and then with acetone. Before electrochemical evaluation, the electrode was dried under vacuum at 100 °C for 12 h. Cell assembly was conducted in a glove box filled with pure argon.

2.3. Basic analysis

The crystal structures of the synthesized powders were examined by X-ray diffraction (XRD) using a Bruker D8 advance diffractometer with filtered Cu kα radiation. The crystalline size was calculated based on the Scherrer equation from the study of the Bragg angle and half bandwidth at the index peak of (1 1 1) plane of $Li_4Ti_5O_{12}$. The particle morphology was examined by Environmental Scanning Electronic Microscope (ESEM, QUANTA-2000) and Transmission Electronic Microscope (JEOL TEM 2011). The specific surface area of the samples was characterized by N_2 adsorption at the temperature of liquid nitrogen using a BELSORP II instrument. Prior to analysis, the samples were treated at 200 °C for 3–5 h in vacuum to remove the surface adsorbed species.

2.4. Electrochemical characterization

The charge–discharge characteristics of the cells were recorded over the potential range between 1.0 and 3.0 V using a NEWARE BTS 5V-50 mA computer-controlled Galvanostat (Shenzhen China) at different rates of 1–40 C at 30 °C. Cyclic voltammetry tests were performed over the potential range of 1.0–3.0 V using a Princeton Applied Research PARSTAT 2273 advanced electrochemical system at the scanning rate of 0.5 mV/s. Complex impedance measurements were carried out using Princeton 2273 electrochemical system over the single cell at the states of fully charged, fully discharged or discharging. A perturbation of 10 mV was applied and data collected under PC control and the frequency range applied is from 1 MHz to 100 mHz.

3. Results and discussion

3.1. Synthesis

The preparation of transparent titanyl nitrate, which ensures the molecular level homogeneous mixing of Li^+ and Ti^{4+} in the precursor stage, was found to be a key point to obtain a pure phase $Li_4Ti_5O_{12}$ during the later calcination. Once tetrbutyl titanate [$Ti(C_4H_9O)_4$] was slowly dropped into de-ionized water, a hydrolysis reaction was occurred via the reaction as described in the following equation:

$$Ti[O(C_4H_9)]_4 + 3H_2O \rightarrow TiO(OH)_2 + 4(C_4H_9)OH \quad (1)$$

Nitric acid was then introduced in time. The formed $TiO(OH)_2$ precipitate was then slowly dissolved by the HNO_3 via the reaction as shown in Eq. (2), until a transparent titanyl nitrate solution (Eq. (2)) was obtained.

$$-Ti-OH + HNO_3 \rightarrow -Ti-NO_3 + H_2O \quad (2)$$

After the impregnation and drying, the solid cellulose–GN precursor still took the morphologic shape of cotton fibers. During the heating treatment at 250 °C, the glycine reacted with nitrates to release a huge amount of heat, which triggered the combustion reaction of the cotton fiber in a following stage. Phenomenally, a sudden formation of enormous amount of gray smoke was happened which lasted less than 30 s, followed by the appearance of smothering combustion with occasional sparks sustained for several minutes. The resulted primary product, easily pulverized, still took the shape of initial cotton fiber while its color changed to gray. It suggests that a large amount of charry organic matters were still presented in the primary product. It was then further calcined between 500 and 900 °C for 5 h in air. After the calcinations at 500 °C, the color turned to bright gray, suggesting minor amount of carbon residual might still be presented in the product. When the calcination temperature was elevated to 700 or 800 °C, the powder took the color of carbon-free white. At 900 °C, the color changed to bright blue, a characteristic color of Li-deficient $Li_4Ti_5O_{12}$. Such deficiency was resulted from the high evaporating pressure of lithium oxide at 900 °C and the stoichiometric ratio of Li and Ti (4/5) applied in the synthesis.

Fig. 2 shows the X-ray diffraction patterns of (a) the cellulose–GN primary product and the samples after the further calcination at various temperatures for 5 h in air, and (b) the samples prepared by the solid-state route. From Fig. 2(a), the primary product is a mixture of $Li_4Ti_5O_{12}$-related phase, anatase-type TiO_2 and rutile-type TiO_2. Very low peak intensity was observed, suggesting their poor crystallinity. After the calcination at 500 °C, the peak intensity of the anatase-type TiO_2 increased significantly. At 600 °C, the main $Li_4Ti_5O_{12}$ phase was formed alongside with the disappearance of the anatase-type TiO_2 phase. At 700 °C, a pure and well-crystallized $Li_4Ti_5O_{12}$ oxide was obtained. Such a low calcination temperature needed to obtain pure phase $Li_4Ti_5O_{12}$ composite oxide suggests the effectiveness of cellulose–GN process for low-temperature synthesis of pure phase $Li_4Ti_5O_{12}$ with good crystallinity. From Fig. 2(b) we can see obviously that using solid-state reaction after calcining at the temperature of 750 °C for 5 h, there is strong peak intensity of rutile-type TiO_2. And it is not pure until the calcined temperature reached 850 °C for 17 h.

The sudden combustion of cellulose–GN precursor within seconds created high temperature about 500 °C as shown in Fig. 3, which facilitated the formation of oxides, while the short combustion time and the prohibited particle contact due to the block effect of cellulose suppressed the crystalline growth during the high-temperature combustion. The cellulose fiber was then burnt out by a following smothering combustion. Since the short combustion time and appropriate combustion temperature for this step, the crystallite size of the oxides did not increase significantly, and the lithium did not lost. Although the auto-combustion did not lead to the formation of the aimed $Li_4Ti_5O_{12}$ phase directly, the small particle size means a short diffusion distance for the following solid-phase reaction; it then allows the synthesis of nano particles with high phase purity after the further calcination at a temperature much lower than

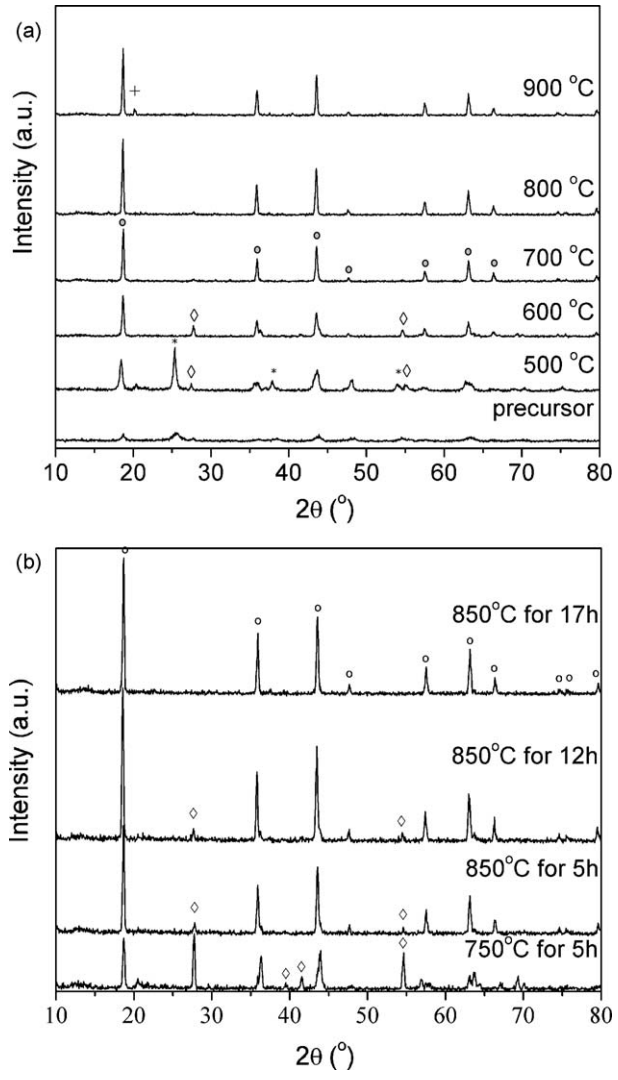

Fig. 2. X-ray diffraction patterns of (a) $Li_4Ti_5O_{12}$ prepared by the cellulose–GN process and calcined further at various temperatures between 500 and 900 °C for 5 h in air; (b) $Li_4Ti_5O_{12}$ prepared by solid-state reaction process (○) Spinel $Li_4Ti_5O_{12}$, (*) anatase TiO_2, (◇) rutile TiO_2, (+) spinel $Li_{1.14}Ti_{1.8}O_4$.

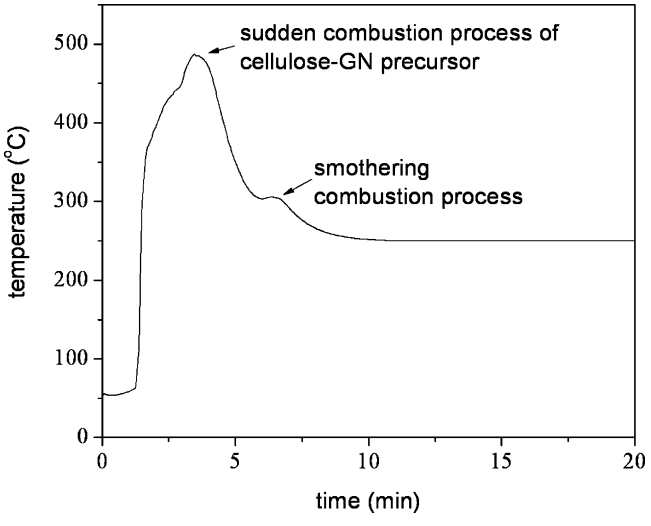

Fig. 3. The temperature–time curve for auto-combustion process of cellulose–GN precursor.

that required based on solid-state reaction and many sol–gel methods [28,45].

Kanamura et al. gained a pure phase of $Li_4Ti_5O_{12}$ at 500 °C by emulsion–gel method [50]. However, a further calcination at 800 °C was necessary to improve the electrochemical performance of the oxide since the low-temperature calcined one had very poor crystallinity, while the electrochemical behavior of $Li_4Ti_5O_{12}$ is typically highly dependent on its crystallinity. Recently, Kavan et al. reported an excellent high rate performance of a nano-crystalline thin-film $Li_4Ti_5O_{12}$ prepared using sol–gel method [21]. As can be seen from their charge/discharge curves the capacity of discharge platform hold less than 50% of the whole discharge capacity. It suggests that a different mechanism from the Li^+ intercalation/de-intercalation in the bulk of $Li_4Ti_5O_{12}$ oxide may play an important role in the charge/discharge process of their nano-powder. The cycling performance, which is of great importance for practical application, is however, also lack for their sol–gel derived anode. In general, a good electrochemical performance of the electrode material requires appropriate particle size and high crystallinity.

As shown in Fig. 2 pure-phase $Li_4Ti_5O_{12}$ was also obtained by cellulose–GN process at a calcination temperature of 800 °C with the peak intensity higher than the 700 °C calcined one, suggesting the improved crystallinity of the oxide with temperature. In addition to the main phase of $Li_4Ti_5O_{12}$, spinel $Li_{1.14}Ti_{1.8}O_4$ impurity phase was also observed after the calcination at 900 °C. It indicates the loss of lithium during this calcination, in accordance with the color change as observed. For the typical solid-phase reaction process, Li_2CO_3 was applied as the raw material, a calcination temperature higher than 800 °C is applied. Since Li_2CO_3 will melt at around 723 °C, the loss of Li by evaporation at temperatures higher than 800 °C is evident. Therefore, excess amount of lithium is typically applied to avoid the lithium deficiency. By the current technique, the spinel $Li_4Ti_5O_{12}$ can be formed at ∼700 °C, which greatly increases the precise stoichiometry of the oxide by effectively avoiding the formation of liquid Li_2CO_3 during the synthesis.

Fig. 4 shows the SEM morphologies of pure cellulose, cellulose–GN precursor, the oxides prepared by further calcination of the primary product (the product from the auto-combustion) at various temperatures between 500 and 900 °C for 5 h in air, and the pure sample prepared by solid-state reaction at 850 °C for 17 h. The dry activated cotton fiber was in a twisted flat tubular shape, while the cotton fiber became round and robust after the impregnation by GN. It suggests that the glycine and metal nitrates successfully soaked into the pores and lumens of the cotton fiber in the cellulose–GN precursor. After the auto combustion and the further calcination at 500–900 °C, the fiber morphological shape was collapsed. With the increase of calcination temperature, the sintering was accelerated. The oxides calcined at 500–700 °C show a porous morphological structure, while large grain with main sizes of 2–5 μm was observed for the sample calcined at 900 °C for 5 h and solid-state reaction at 850 °C for 17 h.

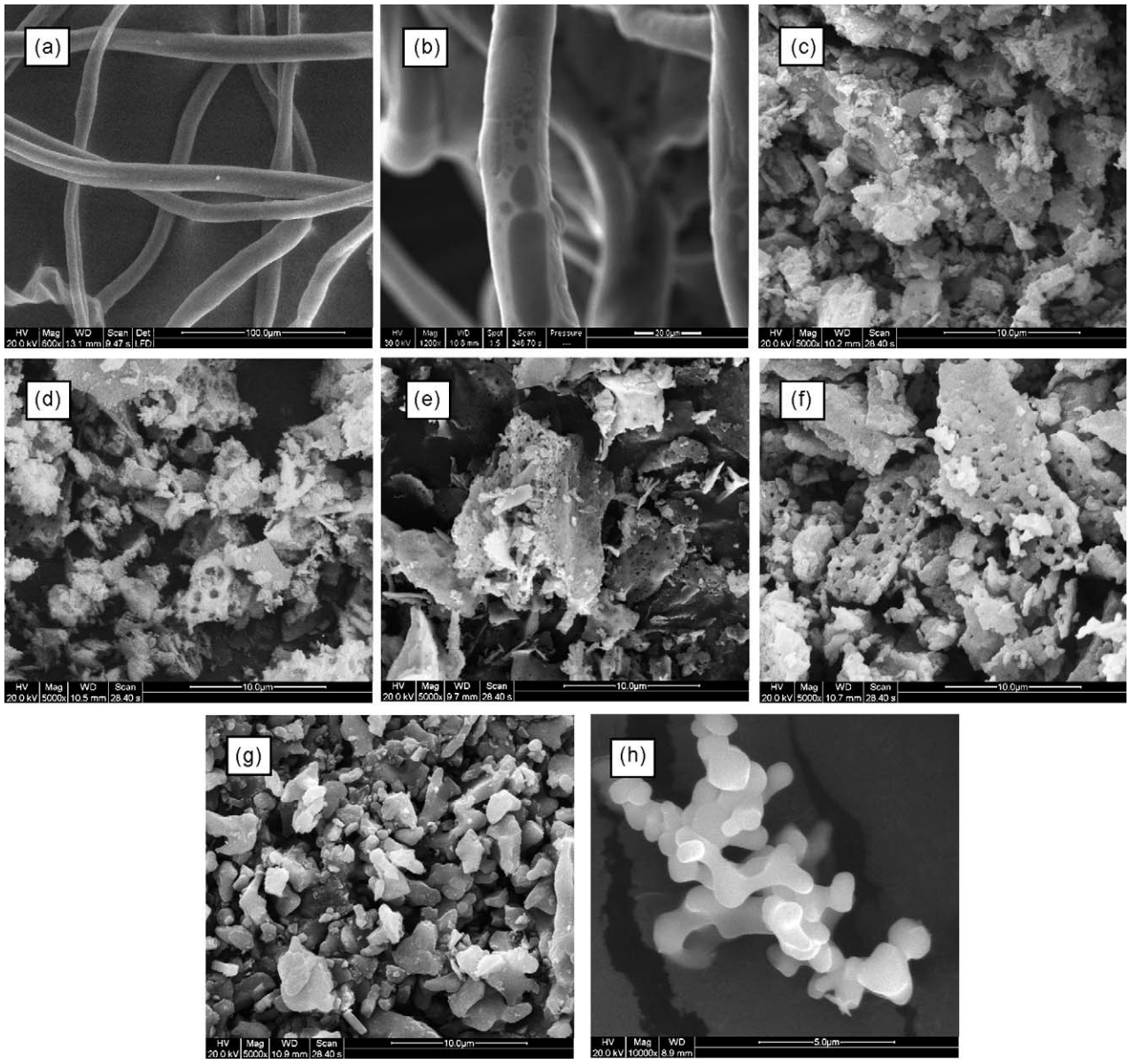

Fig. 4. SEM photos of (a) cellulose, (b) cellulose–GN precursor, and $Li_4Ti_5O_{12}$ prepared by the cellulose–GN process after calcined at various temperatures for 5 h: (c) 500 °C; (d) 600 °C; (e) 700 °C; (f) 800 °C; (g) 900 °C; (h) pure phase of $Li_4Ti_5O_{12}$ prepared by solid-state reaction at 850 °C for 17 h.

The specific surface area and the crystallite size of the cellulose–GN oxide calcined at various calcination temperatures and the pure sample prepared by solid-state reaction at 850 °C for 17 h are listed in Table 1. With the increase of calcination temperature, the particle size increased while the surface area decreased obviously. The particle size of the 700 and 800 °C calcined samples was further examined by TEM. As shown in Fig. 5, the 700 °C calcined one is in quasi-sphere shape with the particle size of 10–20 nm, which increased to 50–100 nm when the calcination temperature is 800 °C.

Table 1
Surface areas, crystalline size and coulombic efficiency of first cycle of the $Li_4Ti_5O_{12}$ anodes prepared from two kinds of methods.

Type of reactions	Cellulose–GN process and calcined for 5 h					Solid-state reaction and calcined for 17 h
Temperature (°C)	500	600	700	800	900	850
Surface area (m^2/g)	9.81	4.59	3.07	1.41	0.52	0.95
Crystallite size* (nm)	22.7	30.6	33.1	36.1	37.8	37.1
Coulombic efficiency of first cycle (%)	60.0	80.9	93.0	92.3	93.8	93.6

* Calculated based on the XRD using Scherrer equation.

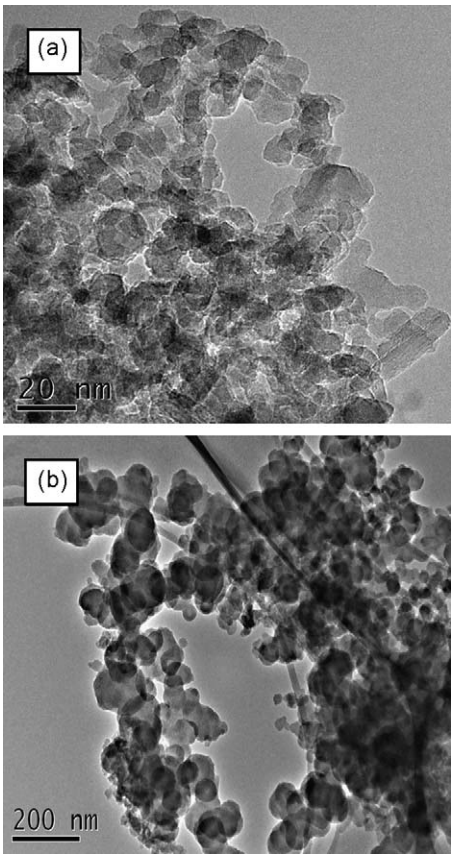

Fig. 5. TEM photos of $Li_4Ti_5O_{12}$ prepared by the cellulose–GN process after calcined various temperatures for 5 h: (a) 700 °C and (b) 800 °C.

3.2. Electrochemical performance

To clarify the effect of impurity on the electrochemical performance of the $Li_4Ti_5O_{12}$, some electrochemical tests were carried. Fig. 6 shows the first discharge/charge curves of the cells with various $Li_4Ti_5O_{12}$ electrodes at 1C rate over the potential range of 1.0–3.0 V, prepared by cellulose–GN process at calcination temperatures between 500 and 900 °C. The first

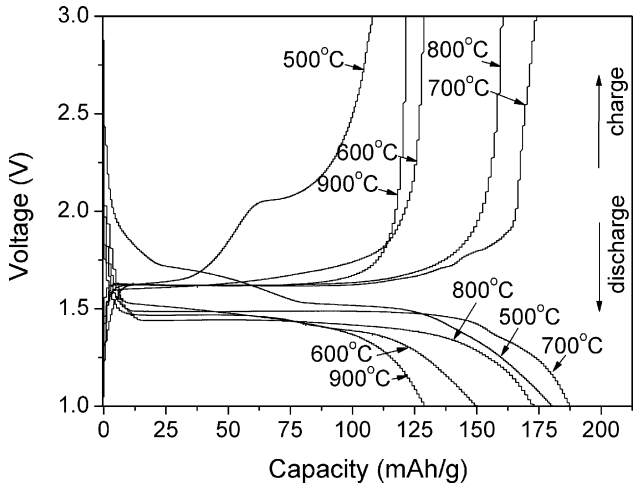

Fig. 6. The first charge–discharge curves for the $Li_4Ti_5O_{12}$ oxides at 1C rate, prepared by cellulose–GN process and calcined between 500 and 900 °C for 5 h.

discharge capacities reached 180.4, 150.1, 187.2, 173.4, and 130.0 mAh/g, respectively, for the anode calcined from 500, 600, 700, 800 and 900 °C. The 500 and 700 °C calcined ones show the initial discharge capacity higher than the theoretical capacity of spinel $Li_4Ti_5O_{12}$ (175 mAh/g), which may be related with the nano-crystalline of the particles, the small amount of carbon residual and high content of impurity phases (for example, large amount of anatase-type TiO_2) as shown in Fig. 2. Kim also observed that nano-size $Li_4Ti_5O_{12}$ had an initial discharge capacity far exceeding its theoretical value [26]. The reversible capacity of the first cycle was found to be greatly influenced by the calcination temperature. As shown in Table 1, the coulombic efficiency for the 1st cycle first increased steadily with the increase of calcination temperature, from a value of only ~60% for the 500 °C calcined sample to ~93% for the 700 °C calcined one, and then kept nearly constant with the further increase of the calcination temperature. However, the irreversible capacity was observed only at the first cycle, i.e., near 100% coulombic efficiency for the following cycles. It is well known that the irreversible capacity on carbon anode is frequently associated with SEI layer formation. Due to the high cut-off voltage (1.0 V) applied in this study for the discharge process; the SEI layer formation is unlikely over the $Li_4Ti_5O_{12}$ electrodes [19,20]. The poor capacity reversibility of the 500 and 600 °C calcined ones may be related with their poor crystallinity and/or possible impurities. Since the Li-ion intercalation and de-intercalation are relied on the stable metal oxide structures of the anode, some intercalated lithium in the first discharge process possibly was not able to be de-intercalated due to the defects in the crystallites. The phase structure of the anode mixture was stabilized after the first cycling, which then led to no further decay of the capacity. At a calcination temperature higher than 700 °C, well-crystallized $Li_4Ti_5O_{12}$ phase was formed. Its irreversible capacity in the first cycle is likely associated with the poor intrinsic electronic conductivity on recharge.

Different from the anodes prepared from the calcination between 600 and 900 °C, which show only one discharge/charge voltage platform at ~1.5 V/~1.6 V, the 500 °C calcined one shows two discharge/charge platforms, one around 1.68 V (~2.07 V) and the other at ~ 1.50 V (~1.65 V). Similarly, two discharge/charge platforms were also observed by Zhang et al. for some microwave synthesized $Li_4Ti_5O_{12}$ [51]. They ascribed the additional discharge/charge platforms to the Li-ion insertion/extraction into/from the anatase TiO_2 impurity phase. As observed in Fig. 2, the 500 °C calcined sample is characterized by the presence of noticeable amount of anatase-type TiO_2. The pure anatase-type TiO_2 was then also investigated as the anode at the discharge/charge rate of 1C. As shown in Fig. 7, broad discharge and charge platforms were observed at the voltages of 1.76 and 1.95 V, respectively. Such results strongly support that the second discharge/charge platforms for the 500 °C calcined sample were originated from the lithium intercalation and de-intercalation into/from the impurity phase of anatase-type TiO_2 in the anode.

The anode performance of $Li_4Ti_5O_{12}$ is closely related with the particle size, particle morphologies, and crystallographic

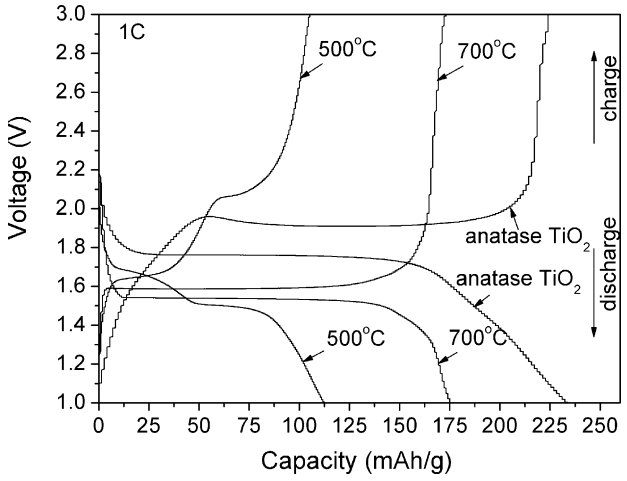

Fig. 7. A comparison of discharge and charge curves of pure $Li_4Ti_5O_{12}$ oxide, anatase TiO_2 and the 500 °C calcined sample prepared from cellulose–GN process.

structure. According to the results in Table 1, with the increase of calcination temperature, the surface area of $Li_4Ti_5O_{12}$ decreased while the crystallite size increased. The larger grain size and smaller surface area means the longer diffusion distance of lithium ion and the smaller surface reaction active sites, which then resulted in the increase of polarization resistance at high charge/discharge rate. On the other hand, since the Li intercalation/de-intercalation into/from $Li_4Ti_5O_{12}$ bulk phase is closely related with its spinel crystallographic structure, a well-crystallized oxide with stable phase structure is required for a high cycling stability and large capacity of an anode. Based on above results, 700–800 °C should be the optimal calcination temperature for high-rate performance of $Li_4Ti_5O_{12}$ anode of this study. The relatively small voltage difference between the charge (1.59 V) and discharge (1.54 V) platforms at 1C rate (Fig. 7) strongly suggests that the 700 °C calcined anode may be a promising material with highly reversible Li-ion intercalation/de-intercalation capability.

Fig. 8 depicts the capability of the $Li_4Ti_5O_{12}$ anodes prepared by cellulose–GN process at calcination temperatures of 700 and 800 °C for 5 h and solid-state reaction at 850 °C for 17 h at high discharge/charge rates of 1–40C. The data was obtained from the second discharge curves. As shown in Fig. 8(a) and (b), excellent high rate-performance was observed for both 700 and 800 °C calcined samples. At a discharge rate of 10C, reversible capacities of ∼125 and 103 mAh/g were observed with near 100% coulombic efficiency, respectively,

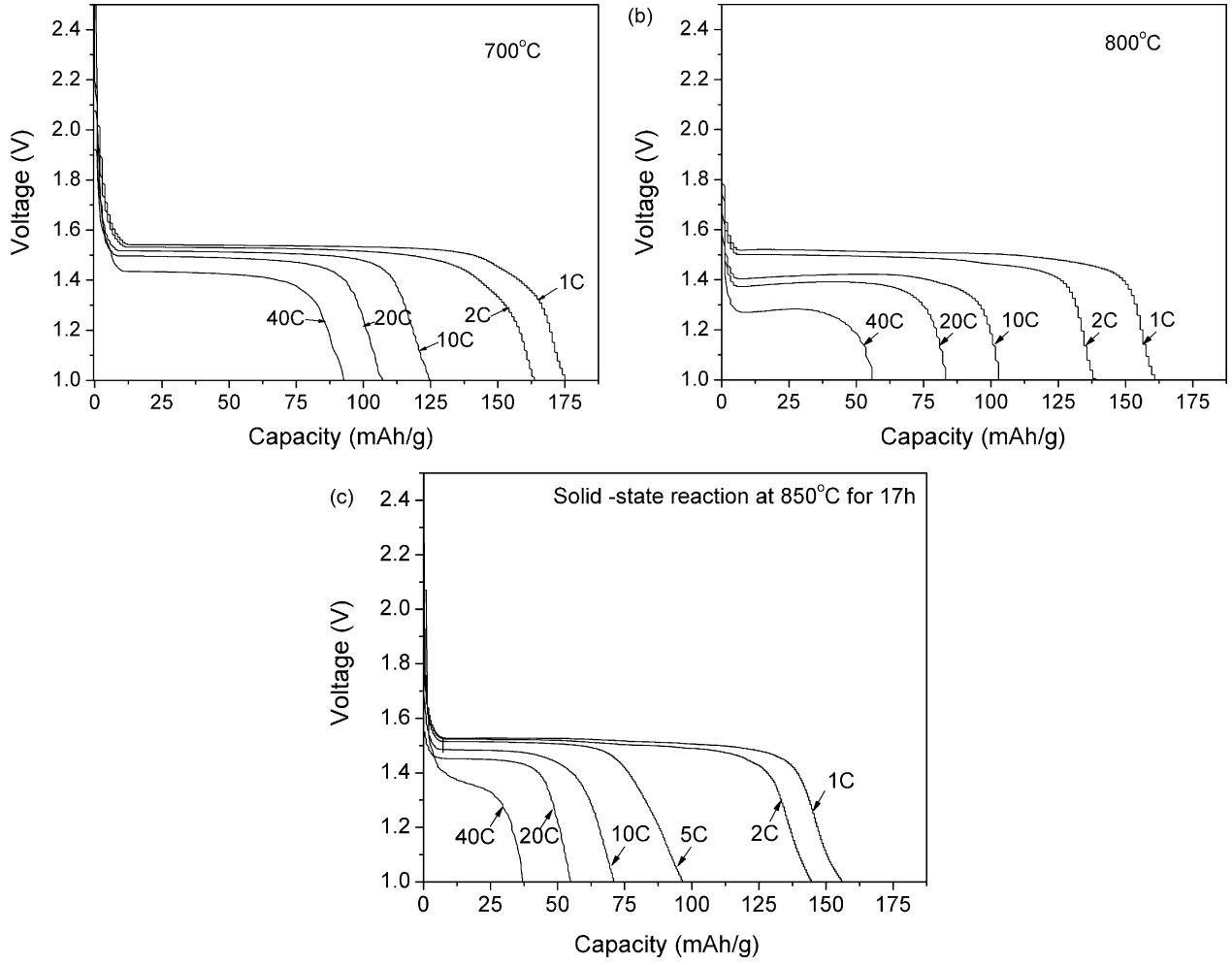

Fig. 8. The discharge profiles for the $Li_4Ti_5O_{12}$ oxides from 1 to 3 V at different rates, prepared from the cellulose–GN process and further calcined at (a) 700 °C for 5 h; (b): 800 °C for 5 h; and (c): solid-state reaction at 850 °C for 17 h.

for the anode calcined at 700 and 800 °C. Even at a discharge rate of 20 C, a high capacity of 108 mAh/g was obtained for the 700 °C calcined sample, while it decreased to around 83 mAh/g for the 800 °C calcined one. Fig. 8(c) displays the rate-capability of solid-state reaction sample. At a low current density, 1C, the sample gained from solid-state reaction at 850 °C for 17 h shows a comparable capacity to the cellulose–GN samples. This should be attributed to the sufficient time for both Li^+ and electronic transport at this low current rate. $Li_4Ti_5O_{12}$ grains inside the agglomerated particles can be electroactive due to long diffusion time. However, with increasing the charge–discharge current rate, the difference between the lithium storage capacities of them becomes evident. The $Li_4Ti_5O_{12}$ powders prepared by cellulose–GN process at calcination temperature of 700 °C for 5 h behave a very slow capacity fading upon increasing the current density. However, the capacity of the solid-state reaction sample drops very rapidly, leaving only 70 mAh/g at 10C and 37.5 mAh/g at 40C. This result is expected because of the smaller crystallite size of $Li_4Ti_5O_{12}$ powders prepared by cellulose–GN process at calcination temperature of 700 °C for 5 h compared to the one prepared by solid-state reaction at 850 °C for 17 h. It is believed that a large portion of the $Li_4Ti_5O_{12}$ grains have become inactive during charge–discharge due to the insufficient Li ion diffusion. This result confirms that the nano-$Li_4Ti_5O_{12}$ oxides obtained by cellulose–GN way can affect the rate-capability of $Li_4Ti_5O_{12}$ anodes.

The charge/discharge platform is an indication of the two-phase mechanism for the Li intercalation and de-intercalation. The capacity of the flat voltage is sometimes more important for practical application. The capacities for the platforms at various discharge rates for the 700 and 800 °C calcined samples are shown in Fig. 9. As compared to the 700 °C calcined one, the 800 °C calcined anode has higher percentage of platform capacity of its overall discharge capacity at discharge rates of 1–20C, which suggests its higher crystallinity, in well accordance with the XRD results. However, the absolute values of capacity for both the platform and the overall discharge for the 800 °C calcined one are lower than that of the

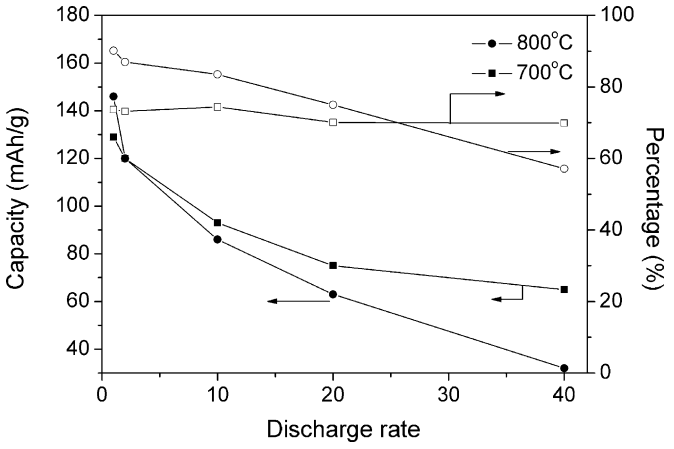

Fig. 9. The capacities for the platforms at various discharge rates for the 700 and 800 °C calcined $Li_4T_5O_{12}$, and the percentage of their corresponding overall discharge capacities.

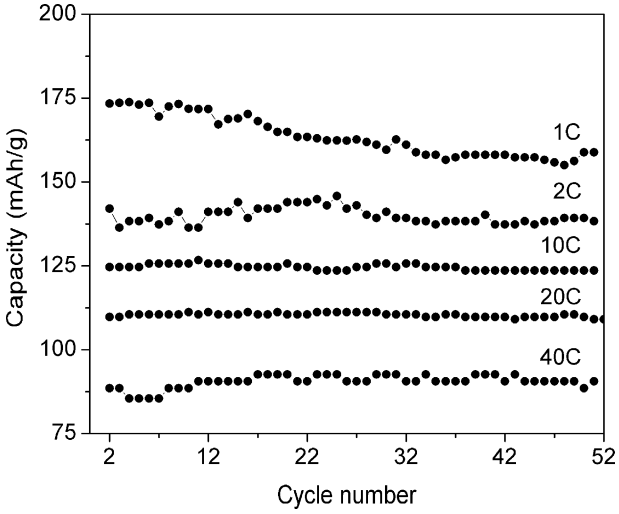

Fig. 10. Variation of the discharge capacities for the 700 °C calcined $Li_4Ti_5O_{12}$ with the cycle number from 1 to 3 V at different discharge rates.

700 °C calcined one at higher discharge rates (10–40C) (Figs. 9 and 10). It suggests that the polarization increased with the calcination temperature. At high charge/discharge rates, large Li^+ ion extraction and insertion fluxes on the anode surface and low Li^+ ion conductivity in the $Li_4Ti_5O_{12}$ bulk resulted in concentration polarization of Li^+ within the electrode materials, which caused the drop of the cell voltage and the termination of the discharge before the maximum capacity of the electrode material is reached. According to the results in Table 1, the higher calcination temperature resulted in a larger crystallite size and smaller surface area. The larger grain size means longer diffusion distance for the lithium ion and electron inside the particle bulk so the larger lithium and electron bulk diffusion resistance, while a smaller surface area means less surface active sites for surface reactions so a larger interfacial polarization resistance. Consequently, the discharge capacity at high discharge rate decreased with the increase of calcination temperature.

The cycling behaviors of the 700 °C calcined $Li_4Ti_5O_{12}$ were investigated. As shown in Fig. 10 is the discharge capacity vs. cycle number for the 700 °C calcined samples at various discharge rates between of 1 and 40C for ~50 times. Stable rate capacity was observed even at 40C, it suggests the promising application of the cellulose–GN method for the synthesis of nano-crystalline powders for high-rate rechargeable lithium battery. Interestingly, the rate capacity decayed slightly in the first 20 cycles at 1C discharge rate. Since it was highly stable even at 40 C, the slight decay at 1C rate is unlikely due to the phase transition of $Li_4Ti_5O_{12}$. It may be associated with the detachment of anode powder from the current collector of the copper film during the operation. At 1C discharge rate, one cycle takes about 120 min, while it takes only 12 min for one complete cycle at 10 C. The much longer time on operation at 1C then greatly increased the possibility of the detaching of active material from the current collector. The improvement of the cell preparation technique to increase the adhesion of the active materials to current collector is then important for

long-term operational stability. More research works are definitely needed.

Fig. 11 shows the cyclic voltammaograms of cells using the 700 °C calcined $Li_4Ti_5O_{12}$ anode at the scanning rate of 0.5 mV/s between 1.0 and 3.0 V, such a scanning rate equals to a charge/discharge rate of ~1C in a galvanostatic charge/discharge process. Only one oxidation/reduction peak is observed. The cathodic peak located around ~1.49 V corresponds to the voltage platform of the discharge process in which Li intercalated into the spinel $Li_4Ti_5O_{12}$. The anodic peak located at ~1.66 V corresponds to the voltage platform of the charge process in which Li de-intercalated from the spinel $Li_7Ti_5O_{12}$. Their difference is about 117 mV, somewhat larger than the difference between charge and discharge rates of 1C (50 mV) (Fig. 5). Such difference may be caused from electrochemical polarization. Since there is no other redox peaks in the cyclic voltammaograms, the spinel $Li_4Ti_5O_{12}$ is pure in nature, in accordance with the XRD results. Except the first cathodic peak which shows larger peak area than the following cycles, the cyclic voltagemmetric curves repeated with each other very well for the cycle 2 to cycle 6. It further supports the high reversibility and stability of the Li-ion intercalation and de-intercalation into/from the 700 °C calcined $Li_4Ti_5O_{12}$ anode.

To further understand the electrode process kinetic behavior, electrochemical impedance spectroscopy measurement was conducted. Fig. 12(a) shows the Nyquist plots of the $Li_4Ti_5O_{12}$|electrolyte|Li cell in the completely discharge (1.0 V), the complete charge (3.0 V) and the first discharge platform (1.54 V) states. The plots are comprised of a depressed semicircle in high-to-medium frequency range and a line inclined at constant angle to the real axis in the frequency range below 5 Hz. The high-frequency intercept at the x axis is typically attributed to the ohmic resistance of the cell (mainly contributed from the electrolyte), while the depressed semicircle in the high-to-medium frequency range is normally related to the complex reaction process over the electrolyte/anode interface, which may also include the

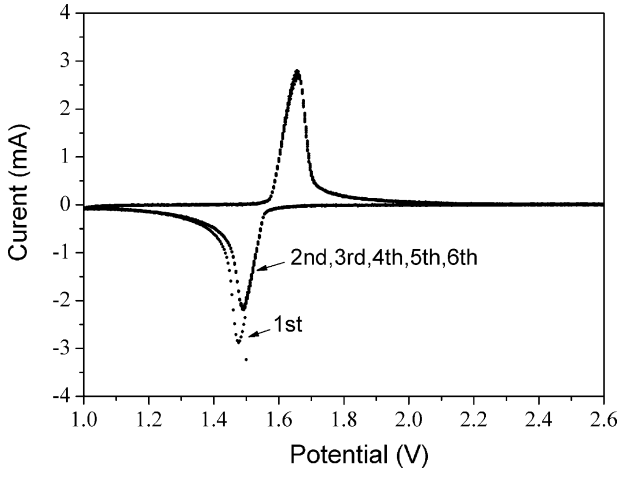

Fig. 11. Cyclic voltammograms of cells using the 700 °C calcined $Li_4Ti_5O_{12}$ at the scanning rate of 0.5 mV/s.

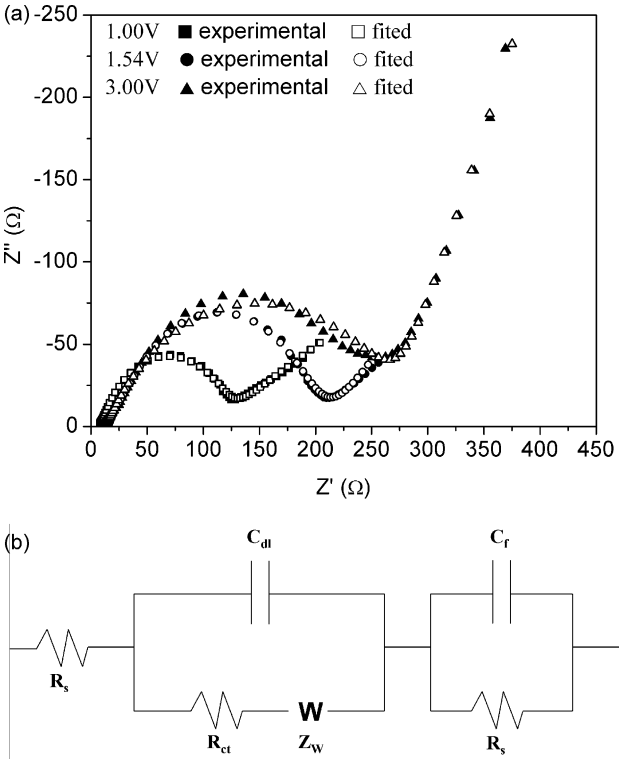

Fig. 12. (a) Complex impedance plots of the half cell with the 700 °C-calcined $Li_4Ti_5O_{12}$ as anode, at the state of totally discharged (1.0 V), charged (3.0 V) and the charging (1.54 V). (b) Equivalent circuit for the Fig. 11. (a) R_s: electrolyte resistance; R_{ct}: change transfer resistance at the surface film-active material interface; R_f: surface polarization resistance; C_{dl}: double-layer capacitance of the electrode–electrolyte interface; C_f: surface capacitance; Z_w: Warburg impedance.

particle to particle contact resistance, charge-transfer resistance and corresponding capacitances. The inclined line in the lower frequency range, attributed to the Warburg impedance, is associated with lithium-ion diffusion through the $Li_4Ti_5O_{12}$ electrode [52,53]. The data of Fig. 12(a) were found to be well fitted by the equivalent circuit as shown in Fig. 12(b). In the equivalent circuit, R_s indicates the ohmic resistance of electrolyte and electrode; R_{ct} is attributed to the charge transfer resistance at the active material interface; R_f is the polarization resistance related with surface charge/discharge process and contacting resistance between anode particles; C_{dl} represents the double-layer capacitance of the electrode–electrolyte interface and C_f indicates the surface capacitance. R_s, R_{ct}, R_f, C_f and C_{dl} all correspond to the high-frequency semicircle. Z_w is the Warburg impedance caused by a semi-infinite diffusion of Li^+ ion in electrode and corresponds to the inclined line in the lower frequency range. As can be seen from Fig. 12 that R_s, R_{ct} and R_f decreased obviously and steadily transition from the fully charge state to the fully discharge state. The total electrode resistances at 1.00, 1.54 and 3.00 V are 124.1, 151.5 and 189.3 Ω, respectively. The reduction ratio reached almost 70%. It suggests that the complex process at the electrolyte/anode interface is greatly improved after the discharging. For the lithium intercalation/de-intercalation through $Li_4Ti_5O_{12}$ anode, it can be expressed

as following equation.

$$(\text{charge}, Ti^{3+} \rightarrow Ti^{4+})Li_4Ti_5O_{12} + 3Li^+ + 3e^- \leftrightarrow Li_7Ti_5O_{12}(\text{discharge}, Ti^{3+} \rightarrow Ti^{4+}) \quad (3)$$

The intercalation/de-intercalation process is associated with the redox of Ti^{4+}/Ti^{3+}. The discharge process resulted in the reduction of Ti^{4+} to $Ti^{3+}$and the increase of the electronic conductivity of the anode [54]. The simultaneous reduction in the size of the high-frequency depleted semi-circle suggests the electrolyte/electrode complex reaction is significantly improved with the increase of the electronic conductivity of $Li_4Ti_5O_{12}$. Such improvement, based on the results in Fig. 12, may be associated with the improvement of the charge transfer process over the electrode surface. Anyway, a surface modification with conductive materials could then be beneficial for further improving the anode performance of the as-synthesized $Li_4Ti_5O_{12}$. The surface modification with higher conductive oxide such as silver, copper, conduction carbon and others indeed resulted in a significant improvement of rate performance of $Li_4Ti_5O_{12}$ [34–38]. Modification of as-synthesized $Li_4Ti_5O_{12}$ with conductive materials to further improve its rate performance will be conducted soon.

The chemical diffusion coefficient of Li^+ inside $Li_4Ti_5O_{12}$ can be estimated from the impedance results. The following expression for Z_w was derived by solving Fick's law [53,55]:

$$Z_w = A\omega^{-1/2} - jA\omega^{-1/2} \quad (4)$$

$$A = \frac{V_M(dE/dx)}{\sqrt{2}zF\tilde{D}^{1/2}a} \quad (5)$$

where, ω is the frequency, $j = \sqrt{-1}$, and the pre-exponential factor A is a constant which contains a concentration independent chemical diffusion coefficient, as shown in Eq. (5). V_M is the molar volume of $Li_4Ti_5O_{12}$ (45.73 cm^3/mol), dE/dx is the slope of the electrode potential curve vs. x in Fig. 13, z is the charge transfer number ($z = 1$ in the lithium intercalation reaction), a is the electroactive surface area of the electrode, which is 0.785 cm^2 in our testing electrode, F is the Faraday constant, and $\tilde{D}$ is the diffusion coefficient.

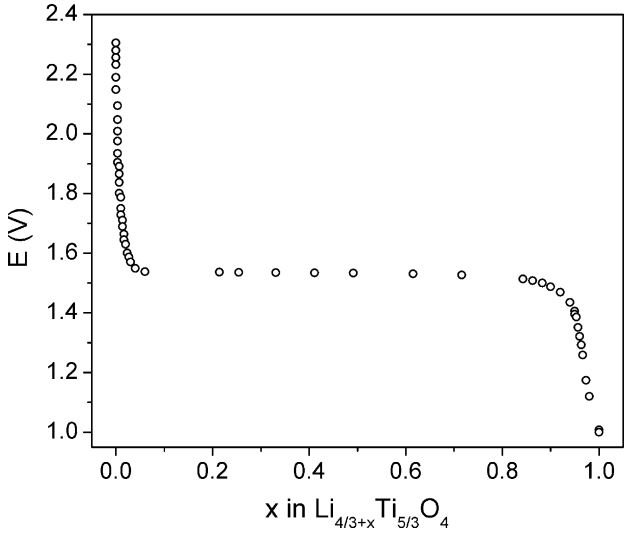

Fig. 13. The relationship of voltage vs. x in $Li_{4/3+x}Ti_{5/3}O_4$ electrode prepared from the cellulose–GN process and further calcined at 700 °C for 5 h.

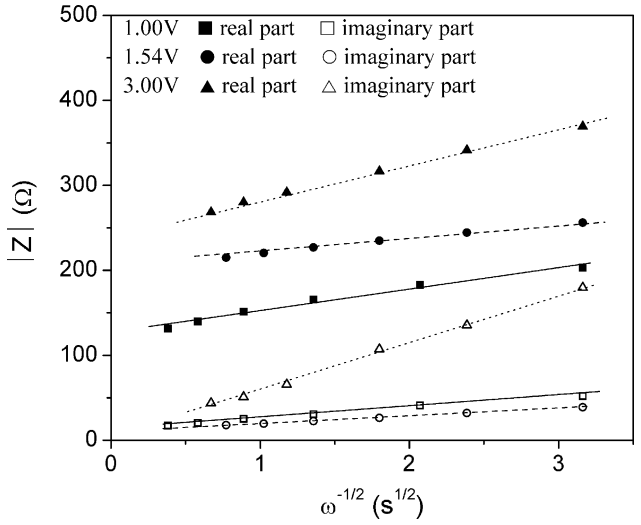

Fig. 14. Real and imaginary parts of the complex impedance vs. $\omega^{-1/2}$ at potentials about 1.00, 1.54 and 3.00 V.

Fig. 14 displays the dependence of impedances on frequencies at the cell potentials of 1.00, 1.54 and 3.00 V. Both the real and imaginary parts of impedance were found to be parallel to each other, and proportional to $\omega^{-1/2}$, in accordance with the result reported by Rho and Kanamura [55]. Based on the slope of the plot, the value of A was obtained. Since A is inversely proportional to the chemical diffusion coefficient, $\tilde{D}$, as demonstrated in Eq. (5), the larger A, the slower diffusion rate of Li^+ ions in the solid matrix of the electrode should be. Table 2 lists the values of dE/dx, A and $\tilde{D}$ at various electrode potentials. The chemical diffusion coefficient, $\tilde{D}$, at around 1.54 V was failed to be obtained as dE/dx almost equal to 0 due to the coexistence of two phases, however, the corresponding A value is the smallest, suggesting the diffusion of Li^+ ions is very fast at such potential vs. Li/Li^+. This conclusion agrees well with the observation of Rho and Kanamura [55]. The chemical diffusion coefficient ranging from 1.98×10^{-8} to 5.43×10^{-9} cm^2/s was observed at 30 °C. A reported value of Li chemical diffusion coefficient inside $Li_4Ti_5O_{12}$ is at the range of 2×10^{-8} to 2×10^{-12} cm^2/s [55,56]. Our results are among the best reported results. The variation of Li^+ diffusion coefficient reported by different researchers suggests that the synthesis technique has significant effect on the Li^+ transportation inside the electrode. On the other hand, the current cellulose-based synthesis technique turns out to be an excellent one for achieving $Li_4Ti_5O_{12}$ oxide with a high Li^+ bulk diffusion coefficient.

Table 2
Values of A, dE/dx and $\tilde{D}$ correspond to the voltage of 1.00, 1.54 and 3.00 V.

Voltage (V)	A	dE/dx	$\tilde{D}$
1.00	25.85	4.46	5.43×10^{-9}
1.54	17.25	→0	—
3.00	40.56	42.25	1.98×10^{-8}

4. Conclusions

Nano-sized spinel $Li_4Ti_5O_{12}$ powders have been successfully synthesized by a novel glycine-nitrate combustion process constricted in the pores of cellulose fibers. The $Li_4Ti_5O_{12}$ powders, which calcined at 700 and 800 °C, have pure phase and good crystallinity with average particle size of ~28 and 60 nm, respectively, smaller than those obtained by solid-state reaction and many sol–gel methods, due to the bock effect of cellulose during the combustion synthesis and the short combustion time. High electrochemical performance was reached for the 700 °C calcined one, which delivered an attractive capacity of ~125 mAh/g at 10C discharge rate with fairly stable cycling performance even at 40C, owing to the good crystallinity and phase purity. The cyclic voltammogram measurement testified that the electrochemical reaction of the prepared $Li_4Ti_5O_{12}$|electrolyte|Li cell has high reversibility and cycling performance. The electrochemical impedance spectroscopy results support that the anode performance is improved when the electronic conductivity was increased. The Li^+ ion is more mobile in the active material near 1.54 V vs. Li/Li^+ corresponding to the two-phase coexistence region. Accordingly, the surface modification of $Li_4Ti_5O_{12}$ with improved surface reaction kinetics could further increase the performance of the resulted $Li_4Ti_5O_{12}$ anode.

Acknowledgements

This work was supported by National Basic Research Program of China under contract no. 2007CB209704. Dr. Zongping Shao also acknowledges the financial support from Chinese Ministry of Education via the Program for Changjiang Scholars and Innovative Research Team in University (no. IRT0732).

References

[1] A.N. Jansen, A.J. Kahaian, K.D. Kepler, P.A. Nelson, K. Amine, D.W. Dees, D.R. Vissers, M.M. Thackeray, Development of a high-power lithium-ion battery, J. Power Sources 81–82 (1999) 902–905.

[2] A.F. Burke, Batteries and ultracapacitors for electric, hybrid, and fuel cell vehicles, Proc. IEEE 95 (2007) 806–820.

[3] K. Takei, K. Ishihara, K. Kumai, T. Iwahori, K. Miyake, T. Nakatsu, N. Terada, N. Arai, Performance of large-scale secondary lithium batteries for electric vehicles and home-use load-leveling systems, J. Power Sources 119–121 (2003) 887–892.

[4] D. Aurbach, E. Zinigrad, Y. Cohen, H. Teller, A short review of failure mechanisms of lithium metal and lithiated graphite anodes in liquid electrolyte solutions, Solid State Ionics 148 (2002) 405–416.

[5] R.M. Dell, Batteries fifty years of materials development, Solid State Ionics 134 (2000) 139–158.

[6] J.M. Tarascon, M. Armand, Issues and challenges facing rechargeable lithium batteries, Nature 414 (2001) 359–367.

[7] K. Zaghib, M. Simoneau, M. Armand, M. Gauthier, Electrochemical study of $Li_4Ti_5O_{12}$ as negative electrode for Li-ion polymer rechargeable batteries, J. Power Sources 81–82 (1999) 300–305.

[8] K. Zaghib, M. Armand, M. Gauthier, Electrochemistry of anodes in solid-state Li-ion polymer batteries, J. Electrochem. Soc. 145 (1998) 3135–3140.

[9] P. Birke, F. Salam, S. Döring, W. Weppner, A first approach to a monolithic all solid state inorganic lithium battery, Solid State Ionics 118 (1999) 149–157.

[10] A.D. Pasquier, A. Laforgue, P. Simon, $Li_4Ti_5O_{12}$/poly(methyl)thiophene asymmetric hybrid electrochemical device, J. Power Sources 125 (2004) 95–102.

[11] S.I. Pyun, S.W. Kim, H.C. Shin, Lithium transport through $Li_{1+\delta}[Ti_{2-y}Li_y]O_4$ ($y = 0$; 1/3) electrodes by analysing current transients upon large potential steps, J. Power Sources 81–82 (1999) 248–254.

[12] E.M. Sorensen, S.J. Barry, H.K. Jung, J.R. Rondinelli, J.T. Vaughey, K.R. Poeppelmeier, Three-dimensionally ordered macroporous $Li_4Ti_5O_{12}$: effect of wall structure on electrochemical properties, Chem. Mater. 18 (2006) 482–489.

[13] T. Ohzuku, A. Ueda, N. Yamamoto, Zero-strain insertion material of $Li[Li_{1/3}Ti_{5/3}]O_4$ for rechargeable lithium cells, J. Electrochem. Soc. 142 (1995) 1431–1435.

[14] T. Ohzuku, K. Ariyoshi, S. Yamamoto, Y. Makimura, 3-volt lithium-ion cell with $Li[Ni_{1/2}Mn_{3/2}]O_4$, Chem. Lett. 30 (2001) 1270–1271.

[15] E. Ferg, R.J. Gummov, A.de. Kock, M.M. Thackeray, Spinel anodes for lithium-ion batteries, J. Electrochem. Soc. 141 (1994) L147–L150.

[16] K.M. Colbow, J.R. Dahn, R.R. Haering, Structure and electrochemistry of the spinel oxides $LiTi_2O_4$ and $Li_{4/3}Ti_{5/3}O_4$, J. Power Sources 26 (1989) 397–402.

[17] Y.H. Rho, K. Kanamura, T. Umegaki, $LiCoO_2$ and $LiMn_2O_4$ thin-film electrodes for rechargeable lithium batteries, J. Electrochem. Soc. 150 (2003) A107–A111.

[18] Y.H. Rho, K. Kanamura, T. Umegaki, Preparation of $Li_{4/3}Ti_{5/3}O_4$ thin film anode with high electrochemical response for rechargeable lithium batteries by sol–gel method, Chem. Lett. 30 (2001) 1322–1323.

[19] P.P. Prosini, R. Mancini, L. Petrucci, V. Contini, P. Villano, $Li_4Ti_5O_{12}$ as anode in all-solid-state, plastic, lithium-ion batteries for low-power applications, Solid State Ionics 144 (2001) 185–192.

[20] D. Peramunage, K.M. Abraham, Preparation of micron-sized $Li_4Ti_5O_{12}$ and its electrochemistry in polyacrylonitrile electrolyte-based lithium cells, J. Electrochem. Soc. 145 (1998) 2609–2615.

[21] L. Kavan, M. Grätzel, Facile synthesis of nanocrystalline $Li_4Ti_5O_{12}$ (spinel) exhibiting fast Li insertion, Electrochem. Solid-State Lett. 5 (2002) A39–A42.

[22] G.G. Amatucci, F. Badway, A.D. Pasquier, T. Zheng, An asymmetric hybrid nonaqueous energy storage cell, J. Electrochem. Soc. 148 (2001) A930–A939.

[23] L. Kavan, M. Grätzel, J. Rathousky, A. Zukal, Nanocrystalline TiO_2 (anatase) electrodes: surface morphology, adsorption, and electrochemical properties, J. Electrochem. Soc. 143 (1996) 394–400.

[24] I. Exnar, L. Kavan, S.Y. Huang, M. Grätzel, Novel 2 V rocking-chair lithium battery based on nano-crystalline titanium dioxide, J. Power Sources 68 (1997) 720–722.

[25] L. Kavan, J. Rathousky, M. Grätzel, V. Shklover, A. Zukal, Surfactant-templated TiO_2 (anatase): characteristic features of lithium insertion electrochemistry in organized nanostructures, J. Phys. Chem. B 104 (2000) 12012–12020.

[26] D.H. Kim, Y.S. Ahn, J. Kim, Polyol-mediated synthesis of $Li_4Ti_5O_{12}$ nanoparticle and its electrochemical properties, Electrochem. Commun. 7 (2005) 1340–1344.

[27] A. Singhal, G. Skandan, G. Amatucci, F. Badway, N. Ye, A. Manthiram, H. Ye, J.J. Xu, Nanostructured electrodes for next generation rechargeable electrochemical devices, J. Power Sources 129 (2004) 38–44.

[28] Y.J. Hao, Q.Y. Lai, Z.H. Xu, X.Q. Liu, X.Y. Ji, Synthesis by TEA sol–gel method and electrochemical properties of $Li_4Ti_5O_{12}$ anode material for lithium-ion battery, Solid State Ionics 176 (2005) 1201–1206.

[29] Y.J. Hao, Q.Y. Lai, J.Z. Lu, H.L. Wang, Y.D. Chen, X.Y. Ji, Synthesis and characterization of spinel $Li_4Ti_5O_{12}$ anode material by oxalic acid-assisted sol–gel method, J. Power Sources 158 (2006) 1358–1364.

[30] S.S. Lee, K.T. Byun, J.P. Park, S.K. Kim, H.Y. Kwak, I.W. Shim, Preparation of $Li_4Ti_5O_{12}$ nanoparticles by a simple sonochemical method, Dalton Trans. 37 (2007) 4182–4184.

[31] Y. Abe, E. Matsui, M. Senna, Preparation of phase pure and well-crystallized $Li_4Ti_5O_{12}$ nanoparticles by precision control of starting mixture and

calcining at lowest possible temperatures, J. Phys. Chem. Solids 68 (2007) 681–686.
[32] J. Kim, J. Cho, Spinel $Li_4Ti_5O_{12}$ nanowires for high-rate Li-Ion intercalation electrode, Electrochem. Solid State Lett. 10 (2007) A81–A84.
[33] J.R. Li, Z.L. Tang, Z.T. Zhang, Controllable formation and electrochemical properties of one-dimensional nanostructured spinel $Li_4Ti_5O_{12}$, Electrochem. Commun. 7 (2005) 894–899.
[34] K. Nakahara, R. Nakajima, T. Matsushima, H. Majima, Preparation of particulate $Li_4Ti_5O_{12}$ having excellent characteristics as an electrode active material for power storage cells, J. Power Sources 117 (2003) 131–136.
[35] L. Cheng, X.L. Li, H.J. Liu, H.M. Xiong, P.W. Zhang, Y.Y. Xia, Carbon-coated $Li_4Ti_5O_{12}$ as a high rate electrode material for Li-ion intercalation, J. Electrochem. Soc. 154 (2007) A692–A697.
[36] S.H. Huang, Z.Y. Wen, J.C. Zhang, X.L. Yang, Improving the electrochemical performance of $Li_4Ti_5O_{12}$/Ag composite by an electroless deposition method, Electrochim. Acta 52 (2007) 3704–3708.
[37] S.H. Huang, Z.Y. Wen, X.J. Zhu, X.L. Yang, Research on $Li_4Ti_5O_{12}/Cu_xO$ composite anode materials for lithium-ion batteries, J. Electrochem. Soc. 152 (2005) A1301–A1305.
[38] G.J. Wang, J. Gao, L.J. Fu, N.H. Zho, Y.P. Wu, T. Takamura, Preparation and characteristic of carbon-coated $Li_4Ti_5O_{12}$ anode material, J. Power Sources 174 (2007) 1109–1112.
[39] Y.J. Hao, Q.Y. Lai, J.Z. Lu, X.Y. Ji, Effects of dopant on the electrochemical properties of $Li_4Ti_5O_{12}$ anode materials, Ionics 13 (2007) 369–373.
[40] Z.M. Zhong, Synthesis of Mo^{4+} substituted spinel $Li_4Ti_{5-x}Mo_xO_{12}$, Electrochem. Solid State Lett. 10 (2007) A267–A269.
[41] S.H. Huang, Z.Y. Wen, Z.H. Gu, X.J. Zhu, Preparation and cycling performance of $Al^{3+}$and F^- co-substituted compounds $Li_4Al_xTi_{5-x}F_yO_{12-y}$, Electrochim. Acta 50 (2005) 4057–4062.
[42] P. Kubiak, A. Garcia, M. Womes, L. Aldon, J. Olivier-Fourcade, P.E. Lippens, J.C. Jumas, Phase transition in the spinel $Li_4Ti_5O_{12}$ induced by lithium insertion Influence of the substitutions Ti/V, Ti/Mn, Ti/Fe, J. Power Sources 119–121 (2003) 626–630.
[43] C.H. Chen, J.T. Vaughey, A.N. Jansen, D.W. Dees, A.J. Kahaian, T. Goacher, M.M. Thackeray, Studies of Mg-Substituted $Li_{4-x}Mg_xTi_5O_{12}$ spinel electrodes ($0 \leq \leq x \leq 1$) for lithium batteries, J. Electrochem. Soc. 148 (2001) A102–A104.
[44] A.D. Robertson, L. Trevino, H. Tukamoto, J.T.S. Irvine, New inorganic spinel oxides for use as negative electrode materials in future lithium-ion batteries, J. Power Sources 81–82 (1999) 352–357.
[45] X.L. Yao, S. Xie, C.H. Chen, Q.S. Wang, J.H. Sun, Y.L. Li, S.X. Lu, Comparisons of graphite and spinel $Li_{1.33}Ti_{1.67}O_4$ as anode materials for rechargeable lithium-ion batteries, Electrochim. Acta 50 (2005) 4076–4081.
[46] M.W. Raja, S. Mahanty, M. Kundu, R.N. Basu, Synthesis of nanocrystalline $Li_4Ti_5O_{12}$ by a novel aqueous combustion technique, J. Alloys Compd. (2008), doi:10.1016/j.jallcom.2007.12.072.
[47] Z.P. Shao, G.X. Xiong, Y.J. Ren, Y. Cong, W.S. Yang, Low temperature synthesis of perovskite oxide using the adsorption properties of cellulose, J. Mater. Sci. 35 (2000) 5639–5644.
[48] Z.P. Shao, G.T. Li, G.X. Xiong, W.S. Yang, Modified cellulose adsorption method for the synthesis of conducting perovskite powders for membrane application, Powder Technol. 122 (2002) 26–33.
[49] W. Zhou, Z.P. Shao, R. Ran, W.Q. Jin, N.P. Xu, Functional nanocomposite oxides synthesized by environmental-friendly auto-combustion within a micro-bioreactor, Mater. Res. Bull. 43 (2008) 2248–2259.
[50] K. Kanamura, T. Chiba, K. Dokko, Preparation of $Li_4Ti_5O_{12}$ spherical particles for rechargeable lithium batteries, J. Eur. Ceram. Soc. 26 (2006) 577–581.
[51] J. Li, Y.L. Jin, X.G. Zhang, H. Yang, Microwave solid-state synthesis of spinel $Li_4Ti_5O_{12}$ nanocrystallites as anode material for lithium-ion batteries, Solid State Ionics 178 (2007) 1590–1594.
[52] X.Z. Liao, Z.F. Ma, Y.S. He, X.M. Zhang, L. Wang, Y. Jiang, Electrochemical behavior of $LiFePO_4$/C cathode material for rechargeable lithium batteries, J. Electrochem. Soc. 152 (2005) A1969–A1973.
[53] C. Ho, I.D. Raistrick, R.A. Huggins, Application of A-C techniques to the study of lithium diffusion in tungsten trioxide thin films, J. Electrochem. Soc. 127 (1980) 343–350.
[54] J. Wolfenstine, U. Lee, J.L. Allen, Electrical conductivity and rate-capability of $Li_4Ti_5O_{12}$ as a function of heat-treatment atmosphere, J. Power Sources 154 (2006) 287–289.
[55] Y.H. Rho, K. Kanamura, Li^+ ion diffusion in $Li_4Ti_5O_{12}$ thin film electrode prepared by PVP sol–gel method, J. Solid State Chem. 177 (2004) 2004–2100.
[56] Y.P. Wu, X.B. Dai, J.Q. Ma, Y.J. Cheng, Lithium-Ion Battery, Applications and Development, Chemical Industry Press, Beijing, 2004, p. 120.